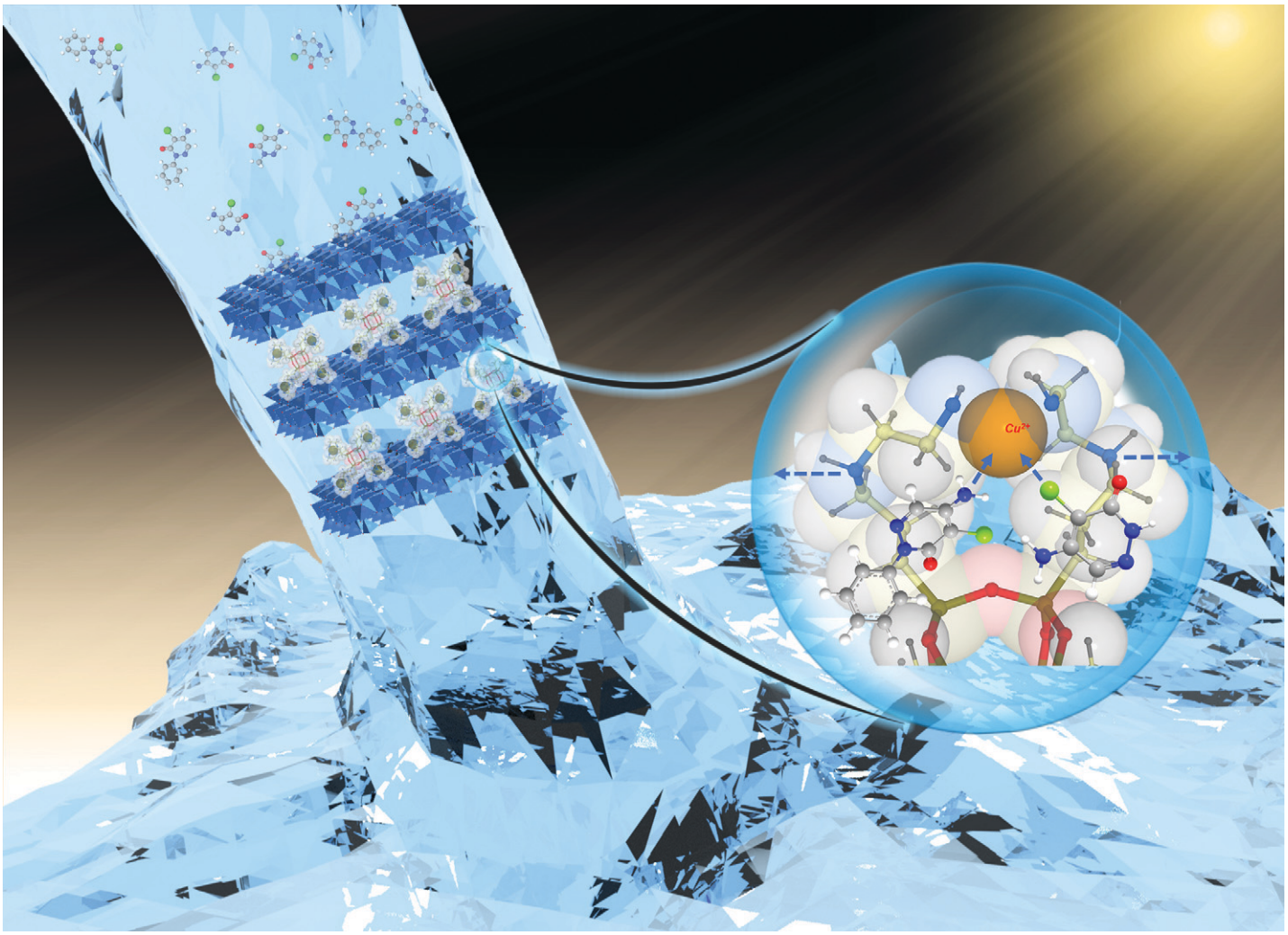

Featuring work from the Surfaces and Thin Films group headed by Prof. Petra Rudolf at the Zernike Institute for Advanced Materials of the University of Groningen, The Netherlands, and the Layered & Nanoporous Materials Group headed by Prof. Dimitrios Gournis at the Department of Materials Science and Engineering of the University of Ioannina, Greece.

Smectite clay pillared with copper complexed polyhedral oligosilsesquioxane for adsorption of chloridazon and its metabolites

Here we propose smectite clay pillared with copper-complexed polyhedral oligosilsesquioxane for the extraction of herbicide residues from drinking water. By choosing appropriate ligands for the polyhedral oligosilsesquioxane and metal ions for the complexation, the material can be adapted to other contaminants.

As featured in:

See Dimitrios Gournis, Petra Rudolf *et al.*, *Environ. Sci.: Nano*, 2020, **7**, 424.

ROYAL SOCIETY OF CHEMISTRY

rsc.li/es-nano

Registered charity number: 207890

Environmental Science Nano

ROYAL SOCIETY OF CHEMISTRY

PAPER

View Article Online
View Journal | View Issue

Check for updates

Cite this: *Environ. Sci.: Nano*, 2020, 7, 424

Smectite clay pillared with copper complexed polyhedral oligosilsesquioxane for adsorption of chloridazon and its metabolites†

Feng Yan, [a] Konstantinos Spyrou, [b] Eleni Thomou, [b] Sumit Kumar, [a] Huatang Cao,[c] Marc C. A. Stuart, [d] Yutao Pei, [c] Dimitrios Gournis *[b] and Petra Rudolf *[a]

Received 28th August 2019,
Accepted 21st November 2019

DOI: 10.1039/c9en00974d

rsc.li/es-nano

Chloridazon has been a widely used herbicide during the past decades, especially in sugar-beet cultivation. UV-induced degradation of chloridazon leads to the formation of desphenyl counterparts, *i.e.* desphenyl-chloridazon and methyl-desphenyl-chloridazon. Even if accumulation of these residues in natural waters is far from alarming, a low-cost effective and environmentally friendly adsorbent, capable of binding chloridazon and its degradation products is desirable to reduce their concentration in water even further below legal limits. Here we show that pillared smectite clay, prepared by cation exchange of sodium with copper complexed, cage-shaped polyhedral oligomeric silsesquioxane (Cu^{2+}@POSS) could be a promising candidate for this purpose. X-ray diffraction and high resolution transmission electron microscopy evidenced a homogeneous layered structure where the interlayer spacing is enlarged by 7.1 ± 0.2 Å (the diameter of Cu^{2+}@POSS) with respect to the pristine clay. Exposure of this pillared smectite clay to chloridazon and its metabolites in water showed that Cu^{2+}@POSS intercalation significantly improved its adsorption capacity. In addition, after several thermal regeneration cycles, Cu^{2+}@POSS_SWy-2 still exhibited excellent adsorption properties. These findings demonstrate that smectite clay pillared with copper complexed polyhedral oligosilsesquioxane is a promising environmentally friendly and relatively low cost material for herbicide waste remediation.

Environmental significance

Chloridazon, a herbicide largely employed in European agriculture, and its metabolites have accumulated in the environment to a level where their elimination from drinking water is recommended to safeguard human health but a recyclable and relatively inexpensive remediation technology for such herbicides has not been developed yet. This work proposes smectite clay pillared with copper-complexed polyhedral oligosilsesquioxane as an adsorbent, and demonstrates the efficacy of this material in extracting chloridazon and its metabolites from water. The design of this adsorbent can be adapted to other contaminants by choosing appropriate ligands for the polyhedral oligosilsesquioxane and metal ions for the complexation as to optimize the pore size and affinity for trapping the chosen molecule.

Introduction

Addressing the lack of adequate and safe water is among the most important challenges in the last few decades.[1] Groundwater, an important source of drinking water in most countries, has been threatened by herbicide/pesticide contamination due to runoff from the soil surface and plants to rivers and lakes.[2] Studies on groundwater contamination have reported increasing amounts of herbicides/pesticides and their metabolites.[3,4] Chloridazon, a selective systemic herbicide used for the control of annual broadleaf weeds, has been widely employed especially in sugar-beet cultivation since it was considered to be a relatively non-harmful herbicide.[5] Its degradation leads to the formation of

[a] *Zernike Institute for Advanced Materials, University of Groningen, Nijenborgh 4, 9747AG Groningen, The Netherlands. E-mail: p.rudolf@rug.nl*
[b] *Department of Materials Science and Engineering, University of Ioannina, 45110 Ioannina, Greece*
[c] *Engineering and Technology Institute Groningen, University of Groningen, Nijenborgh 4, 9747AG, The Netherlands*
[d] *Groningen Biomolecular Sciences and Biotechnology Institute, University of Groningen, Nijenborgh 7, 9747AG Groningen, The Netherlands*

† Electronic supplementary information (ESI) available: XPS survey spectrum of Cu^{2+}@POSS_SWy-2 and pore size distribution of SWy-2, POSS_SWy-2 and Cu^{2+}@POSS_SWy-2 determined by the non-local density functional theory; N1s XPS spectrum of Cu^{2+}@POSS_SWy-2 after adsorption of chloridazon. See DOI: 10.1039/c9en00974d

desphenyl-chloridazon and methyl-desphenyl-chloridazon;[6] the former, produced by aerobic degradation in soil, is predominant. According to European regulations, the maximum residue limit for herbicides is 0.1 μg L^{-1} for single compounds and 0.5 μg L^{-1} for the sum of all herbicides.[7] As reported by Schuhmann *et al.*,[8] in some parts of Europe, chloridazon was detected at concentrations up to 3.5 μg L^{-1}, whereas the metabolites desphenyl-chloridazon and methyl-desphenyl-chloridazon were present in concentrations of 24.0 μg L^{-1} and 6.1 μg L^{-1}, respectively.

In order to limit exposure to chloridazon and its metabolites, their elimination from natural water by the use of an innovative adsorbent with high selectivity and sorption capacity, but available at a relatively low cost, would be an important step forward.[9] Since the beginning of civilization, natural clay minerals have been employed by mankind and because of their low cost, abundance in most continents, high sorption properties and potential for ion exchange, clay materials are also a good option for the present purpose.[10,11] Due to their layered structure, clay materials can host adsorbates and counter ions in the space between the platelets. They exhibit a strong affinity for both cationic and anionic moieties, whereas their sorption capacity for basic molecules is much higher than that for acidic ones because of the negative charge inherent in the clay structure.[12] However, not solely the chemical affinity of the interlayer space of clay can limit the adsorption capacity for chloridazon, but also the size of the interlayer space plays an important role and it is therefore crucial to modify the structure of the clay in order to improve its adsorption capacity.

Pillaring is a well-known technique for engineering the interlayer space in clay materials by increasing the specific surface area and providing accessible, active sites for adsorption.[13,14] Molecules,[15] ions,[16] or complexes[17] can be used as pillaring agents. Among them, organic–inorganic cage-like polyhedral oligomeric silsesquioxanes (POSS) are particularly flexible[18,19] because different organic ligands can tune the functionalization to achieve desired properties. Moreover, the chemical affinity of the nanopores created by pillaring with POSS can be tailored through complexation of metal ions.[20,21]

In this work, we report the intercalation of Cu^{2+}-complexed POSS into smectite clay towards the synthesis of a novel type of pillared structure suitable for environmental remediation. Copper was chosen as a complex metal because of its affinity for nitrogen-containing groups which shows potential for enhancing the adsorption capacity for chloridazon and its metabolites. POSS was selected because it presents three important advantages: i) the eight nitrogen containing organic ligands (–NH_2 and –NH) on each POSS allow complexation of 4 Cu ions; ii) POSS′ cubic shape separates the complexed copper ions from each other and avoids aggregation during the synthesis process, which would reduce the activity of copper ions, and iii) provides the appropriate interlayer space between the smectite layers and the right porosity for chloridazon to interact.

Characterization of the nanocomposite included X-ray diffraction (XRD), high-resolution transmission electron microscopy (HRTEM), scanning electron microscopy (SEM), Fourier transform infrared spectroscopy (FTIR), nitrogen adsorption–desorption measurements, thermogravimetric and differential thermal analysis (TGA/DTA) and X-ray photoelectron spectroscopy (XPS). The pillared clay exhibited a high specific surface area; compared to pristine smectite clay, it showed significant enhancement of adsorption capacity for chloridazon and its metabolites.

Experimental

Materials

Wyoming montmorillonite (SWy-2, $(Na, Ca)_{0.3}(Al, Mg)_2Si_4O_{10}(OH)_2{\cdot}n(H_2O)$), with a cation exchange capacity (CEC) of 78 meq/100 g and flake size of ~200 μm, was obtained from the Source Clay Minerals Repository, Columbia. 3-(2-Aminoethylamino)-propyltrimethoxysilane (EDAPTMOS) was acquired from Fluka Chemicals, chloridazon ($C_{10}H_8ClN_3O$, AR) from Sigma-Aldrich, desphenyl-chloridazon ($C_4H_4ClN_3O$, AR) and methyl-desphenyl-chloridazon ($C_5H_6ClN_3O$, AR) from Enamine Ltd. All the chemicals were used as received.

Synthesis of the Cu^{2+}@POSS_SWy-2 nanocomposite

Milli-Q water (resistivity 18 MΩ cm, 25 °C) was used in the synthesis. SWy-2 was purified with the standard method in clay science, as described in our previous paper.[22] Sodium exchanged montmorillonite was prepared by immersing the pristine clay in 1 N sodium chloride solution, washing it with distilled deionized water and transferring it to dialysis tubes in order to obtain chloride-free clay.[22] The synthesis of cage-shaped POSS was based on a hydrolytic polycondensation reaction; EDAPTMOS was diluted in ethanol/water (v/v = 14/1) to give a 0.45 M POSS solution, which was shaken for a few minutes before bottling for further use.[23,24] 20 mL of 0.15 M $CuCl_2$ aqueous solution (3 mmol) was complexed with 14 mL POSS solution (6 mmol) through sonication and stirred for 30 min. The complexation of the copper cations with the amino and imino groups on the R branches of POSS was evident from the colour change of the complex solution, which turned from light blue to dark blue. The Cu^{2+}@POSSS_SWy-2 nanocomposite was prepared by cation exchange of sodium with copper-complexed POSS (Cu^{2+}@POSS) as indicated in Scheme 1. A suspension of 0.5 wt% SWy-2 in water was mixed with Cu^{2+}@POSS in a weight ratio [Cu^{2+}@POSS]/[SWy-2] = 3, which ensures that there are sufficient siloxane complexes to exchange for the sodium ions in the clay interlayer space. After stirring for 24 h, the Cu^{2+}@POSS_SWy-2 nanocomposite was separated by centrifugation at 5000 rpm and washed three times with ethanol/water (v/v = 1 : 1), before being spread on glass plates for air drying.

In order to study the role of Cu^{2+}, the POSS-pillared clay without the complex metal was also prepared by the same

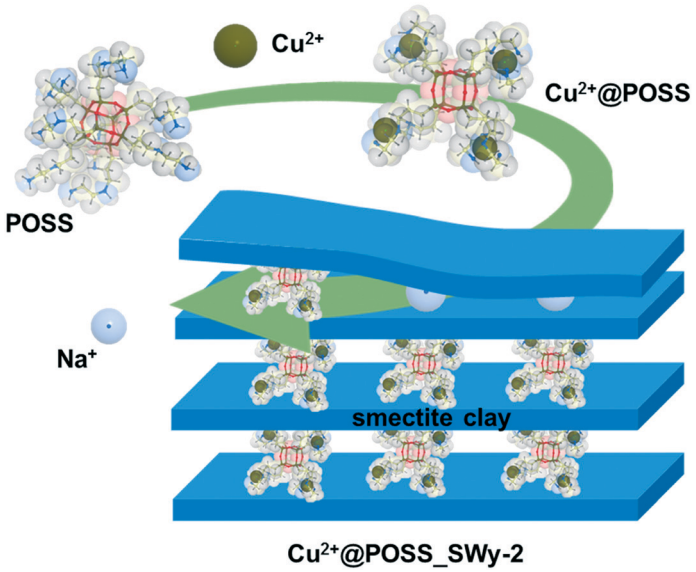

Scheme 1 Schematic representation of the complexation of POSS with Cu^{2+}, and of the intercalation of the POSS complex into the inter-lamellar space of the smectite clay.

synthetic route; this nanocomposite will be identified as POSS_SWy-2 in the following.

Characterization of the pillared nanocomposite Cu^{2+}@POSS_SWy-2

FTIR spectra were recorded on a SHIMADZU 8400 infrared spectrometer in the range of 4000–500 cm^{-1}; each spectrum was the average of 200 scans, collected with a resolution of 2 cm^{-1}. The samples were KBr pellets that contained 2 wt% Cu^{2+}@POSS_SWy-2. XRD spectra were acquired using a D8 Advance Bruker diffractometer with Cu Kα radiation (λ = 1.5418 Å) employing a 0.25° divergent slit and a 0.125° anti-scattering slit; the patterns were recorded in the 2θ range from 2° to 80°, in steps of 0.02° and a counting time of 2 s per step. The nitrogen adsorption–desorption isotherms were measured at −196 °C on a Micromeritics ASAP 2420 V2.05 (V2.05J) porosimeter. Prior to analysis, all three samples were degassed overnight at 120 °C under vacuum. The specific surface area was evaluated with the Brunauer–Emmett–Teller (BET) model by fitting the N_2 adsorption isotherms, the pore volume was determined at P/P_0 = 0.995 and the non-local density functional theory (NLDFT) method[25] was applied to the N_2 adsorption data to obtain the pore size distribution. TGA/DTA was performed using a Perkin Elmer Pyris Diamond TG/DTA. Samples of approximately 5 mg were heated in N_2 from 25 °C to 700 °C, at a rate of 5 °C min^{-1}. TEM images were obtained by using an FEI Tecnai T20, operating at 200 keV. Images were recorded under low-dose conditions with a slow-scan CCD camera. SEM images were recorded with an FEI-Philips FEG-XL30s microscope, and energy dispersive X-ray spectroscopy (EDS) was also performed with the help of an EDAX Octane silicon drift detector with an accelerating voltage of 20 kV. XPS was performed with an SSX-100 (Surface Science Instruments) spectrometer equipped with a monochromatic AlKα X-ray source ($h\nu$ = 1486.6 eV). The measurement chamber pressure was maintained at 1×10^{-9} mbar during data acquisition; the photoelectron take-off angle was 37° with respect to the surface normal. The samples were dispersed in ethanol/water (v/v = 30/70) by sonication and stirring for 30 min, and a small drop of the suspension was left to dry in air on a homemade[26] 150 nm thick gold film supported on mica. Spectral analysis included Shirley background subtraction and fitting with peak profiles taken as a convolution of Gaussian and Lorentzian functions, with the help of the least squares curve-fitting program WinSpec (LISE, University of Namur, Belgium). Binding energies (BEs) were referenced to the Si2p peak[27] at 103.3 eV and are accurate to ±0.1 eV when deduced from the fitting procedure. All measurements were carried out on freshly prepared samples; three different spots were measured on each sample to check for homogeneity.

Batch adsorption experiments

10 mg of Cu^{2+}@POSS_SWy-2, POSS_SWy-2 or SWy-2 was swelled in 10 mL ethanol/water (30/70, v/v) for 24 h under stirring and sonication in a glass vial. Stock solutions of 50 ppm chloridazon, desphenyl-chloridazon and methyl-desphenyl-chloridazon were prepared in ethanol/water (30/70, v/v). Batch adsorption experiments were conducted at ambient temperature. Chloridazon, desphenyl-chloridazon or methyl-desphenyl-chloridazon was added, at concentrations adjusted from 5 ppm to 25 ppm, to 10 mg of swelled suspensions of Cu^{2+}@POSS_SWy-2, POSS_SWy-2 or SWy-2; the suspensions were stirred for 24 h. After the adsorption equilibrium was reached, the suspensions were centrifuged and filtered with 0.45 μm nylon filters. The concentrations of

the herbicide and its metabolites were measured with high performance liquid chromatography (Prominence HPLC, Shimadzu) using a diode array detector and data station and analysed at 283 nm, the wavelength of maximum absorption of these compounds. All of the experimental data reported were the average of triplicate determinations. The adsorption capacities of the organic solute by Cu^{2+}@POSS_SWy-2, POSS_SWy-2 and SWy-2 were calculated with the equation:

$$Q_e = [(C_0 - C_e)/m] \times V \quad (1)$$

where C_0 and C_e are the initial and the adsorption equilibrium concentrations, respectively; m is the mass of the adsorbent and V represents the volume of the suspension.

The adsorption isotherms were analysed with the Freundlich isotherm model, commonly used for aqueous phase adsorption:

$$\ln Q_e = \ln K_f + \frac{1}{n} \ln C_e \quad (2)$$

where K_f represents the Freundlich constant, n is the Freundlich linearity index and C_e represents the adsorption equilibrium concentration.

Thermal regeneration experiments

250 mg of Cu^{2+}@POSS_SWy-2 was added to 250 mL ethanol/water (30/70, v/v) in a glass vial and stirred for 24 h. Stock solutions of 50 ppm chloridazon were prepared in ethanol/water (30/70, v/v). 250 mL of the stock solution of chloridazon was added to the Cu^{2+}@POSS_SWy-2 suspension and the mixture was stirred for 24 h. The adsorbent was separated by centrifugation and dried in an oven (Thermol Scientific Heraeus) overnight at 40 °C, followed by heating in a different oven (Nabertherm box furnace) at 290 °C for 4 h. After that, the cooled sample was carefully weighed and used for the second cycle. Adsorption experiments were carried out with an adsorbent concentration of 0.5 mg mL^{-1} and a chloridazon concentration of 25 mg L^{-1}; four cycles were performed.

Results and discussion

Material characterization

The samples were analysed by FTIR to confirm the successful incorporation of the POSS derivative in the layered structure. The spectra of pristine SWy-2, POSS_SWy-2 and Cu^{2+}@POSS_SWy-2 are shown in Fig. 1(a). One recognizes the characteristic peaks of the smectite clay at 1060 cm^{-1} (Si–O stretching), 695 cm^{-1} and 642 cm^{-1} (Si–O–Si bending vibrations).[28] In addition, in the spectrum of pristine SWy-2, the –OH stretching vibration around 3630 cm^{-1} is ascribed to the presence of –OH on the aluminosilicate skeleton, while the stretching modes at 3400–3600 cm^{-1} and the bending vibration at 1645 cm^{-1} can be attributed to physisorbed

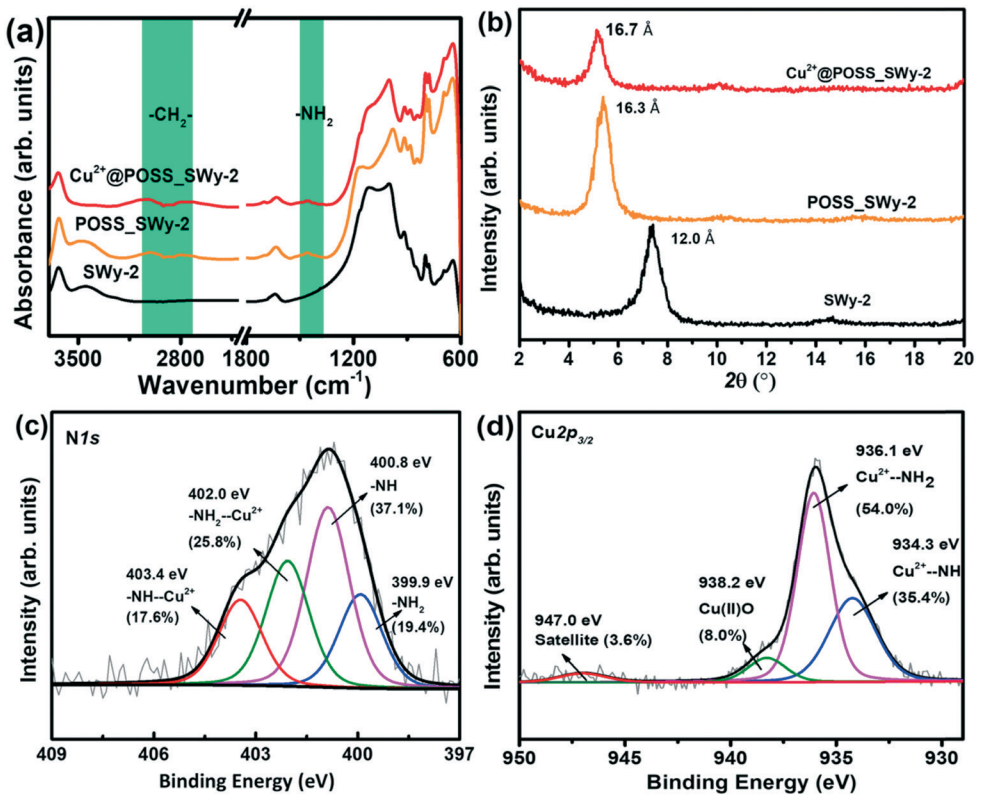

Fig. 1 (a) FTIR spectra and (b) XRD spectra of SWy-2, POSS_SWy-2 and Cu^{2+}@POSS_SWy-2; X-ray photoelectron spectra of Cu^{2+}@POSS_SWy-2 (c) N1s and (d) $Cu2p_{3/2}$ core level regions.

water. A confirmation of the presence of POSS in the hybrid material comes from the bands centred at 2863 cm^{-1} and 2921 cm^{-1}, which correspond to C–H stretching vibrations, as well as from the peak at 1520 cm^{-1}, due to the N–H stretching mode.[29]

The successful intercalation of POSS derivatives in SWy-2 can be proved by XRD, which allows estimation of the interlayer distance between the clay platelets. The XRD spectra of SWy-2, POSS_SWy-2 and Cu^{2+}@POSS_SWy-2 are shown in Fig. 1(b). By applying the Bragg equation, one can derive the basal d_{001}-spacing, which in the pristine smectite clay amounts to 12.0 ± 0.3 Å, but becomes 16.3 ± 0.3 Å after intercalation with POSS. The latter basal plane spacing corresponds to an interlayer separation Δ = (16.3 ± 0.3) Å − 9.6 Å = 6.7 ± 0.3 Å, where 9.6 Å represents the thickness of a single clay layer.[30] This value is in accordance with the size of POSS.[30] For Cu^{2+}@POSS_SWy-2, the basal plane spacing is even larger, namely 16.7 ± 0.4 Å, and the corresponding interlayer separation of (16.7 ± 0.2) Å − 9.6 Å = 7.1 ± 0.2 Å points to successful Cu^{2+} complexation with POSS and intercalation of Cu^{2+}@POSS between the smectite clay layers.[31]

To verify the presence and integrity of Cu^{2+}@POSS within the layered nanostructure, as well as to analyse the chemical environment of Cu^{2+} and POSS, we employed XPS. The overview spectrum attests to the presence of all the expected elements (see ESI,† Fig. S1). The XPS spectrum of the N1s core level region of Cu^{2+}@POSS_SWy-2, shown in Fig. 1(c), shows four contributions in the fit: the spectral signatures of $-NH_2$ and –NH bonds of the POSS are centred at BEs of 399.9 eV and 400.8 eV, respectively, and make up 19.4 ± 4% and 37.1 ± 3% of the total N1s intensity. The contributions at BEs of 403.4 eV and 402.0 eV are respectively due to NH–Cu^{2+} and NH_2–Cu^{2+} and represent 17.6 ± 4% and 25.8 ± 3% of the total N1s intensity. Hence the spectral intensities of the total amounts of $-NH_2$ ($-NH_2$ and $-NH_2$–Cu^{2+}) and –NH– (–NH– and –NH–Cu^{2+}) are almost equal (45.2 ± 2% and 54.7 ± 2%, respectively), which dovetails with the ratio of the two kinds of amino groups in EDAPTMOS. The fact that the spectral intensity of $-NH_2$–Cu^{2+} is higher than that of –NH–Cu^{2+} implies that $-NH_2$ exhibits a stronger affinity for Cu^{2+}.

The XPS spectrum of the $Cu2p_{3/2}$ core level region of Cu^{2+}@POSS_SWy-2 is shown in Fig. 1(d), where the contributions at BEs of 934.3 eV, 936.1 eV and 938.2 eV correspond respectively to the electron-rich NH group Cu^{2+}–NH, the relatively electron-poor amino Cu^{2+}–NH_2 and Cu(II)O; the small peak at 947.0 eV is the shake-up satellite.[32,33] The ratio between Cu^{2+}–NH and Cu^{2+}–NH_2 in the $Cu2p_{3/2}$ spectrum agrees with the N1s spectrum. Taken together, the XPS spectra confirm that Cu^{2+}@POSS was successfully intercalated into SWy-2.

Undeniable proof for the successful intercalation of Cu^{2+}@POSS into the interlayer space of SWy-2 is provided by the high-resolution transmission electron microscopy (HRTEM) images shown in Fig. 2, where the layered structure can be clearly observed in panel (a). The interlayer spacing can be retrieved by performing a fast Fourier transform (FFT) of the image, where the diffraction corresponding to the (001) planes of the SWy-2 structure is observed as shown in Fig. 2(b). Performing an inverse FFT on the marked area, the basal plane spacing d_{002} is measured to be ~1.79 nm in agreement with the XRD result discussed above.

In order to gain further insight into the morphology of the composite material, SEM was performed. A well-defined porous structure, which resembles the crumpled sheet, can be observed on the image in Fig. 3(a). In an enlarged view of the same spot, presented in Fig. 3(b), the exfoliated layers (white arrows) and the enlarged interlayer space (yellow arrows) of the smectite clay can be clearly seen.

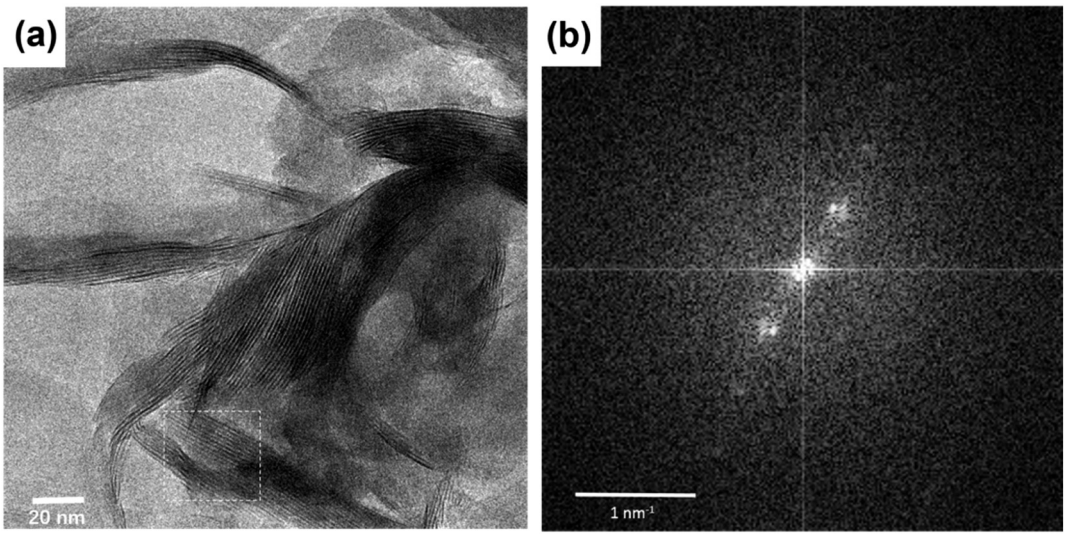

Fig. 2 (a) TEM image of Cu^{2+}@POSS_SWy-2. (b) Fast Fourier transform (FFT) of the square marked in white. An interlayer distance of 17.9 Å is deduced from this graph.

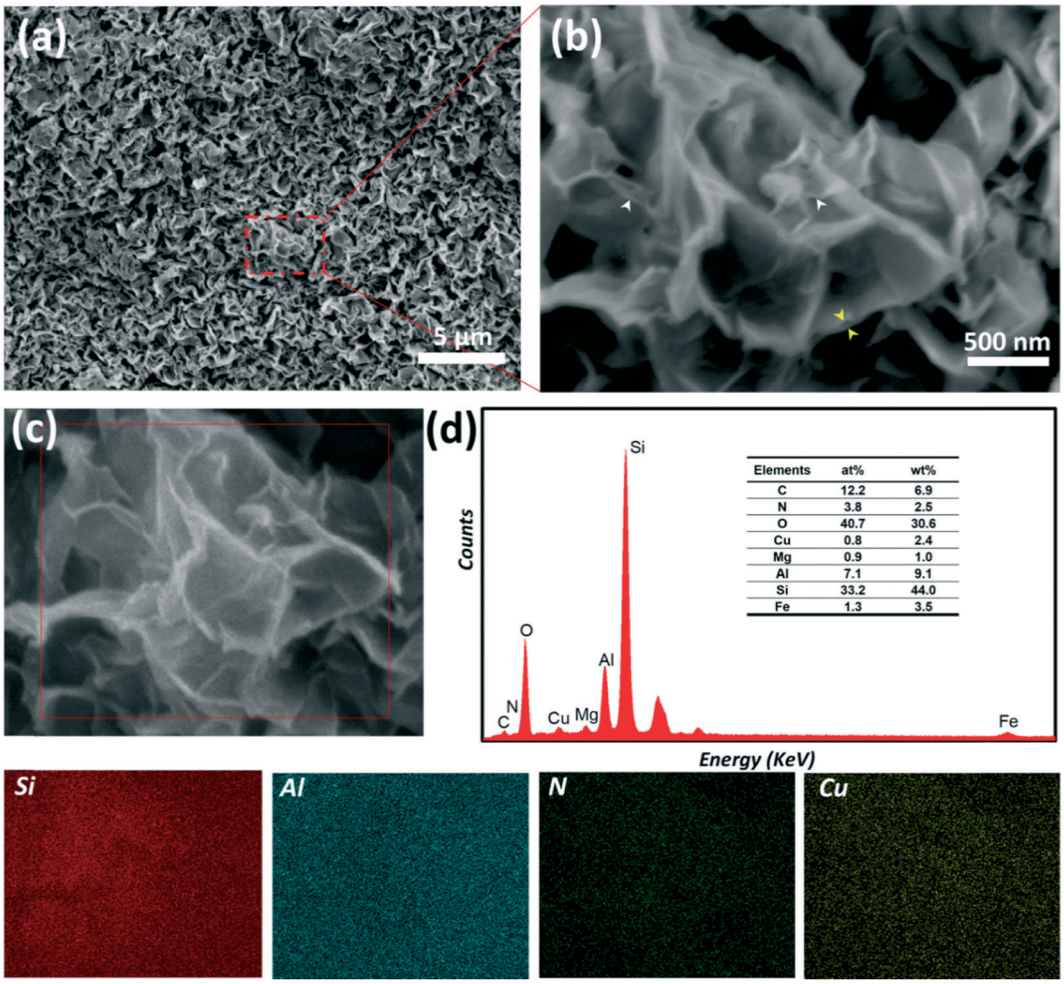

Fig. 3 (a) and (b) SEM images of Cu^{2+}@POSS_SWy-2. (c) SEM image with the area selected for energy dispersive X-ray spectroscopy (EDS) spectra and EDS elemental mapping measurement marked in red. (d) SEM-EDS spectra of Cu^{2+}@POSS_SWy-2. Inset: The elemental composition results. The bottom panels show the EDS elemental mapping results for Si, Al, N and Cu in Cu^{2+}@POSS_SWy-2 based on the red square area in (c).

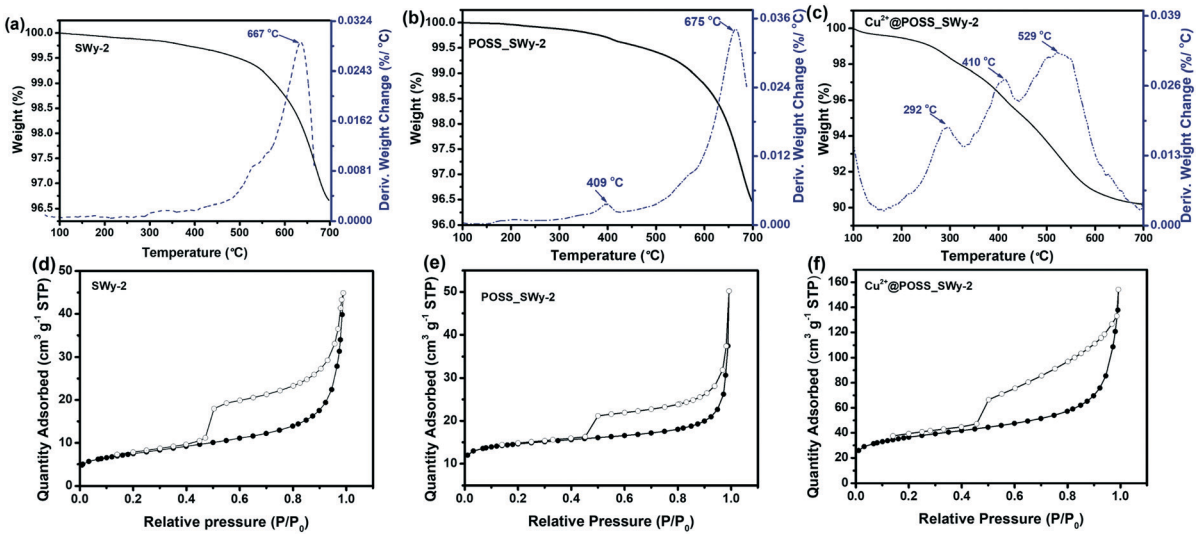

Fig. 4 Thermogravimetric analysis (TGA) and differential thermal analysis (DTA) data for (a) SWy-2, (b) POSS_SWy-2 and (c) Cu^{2+}@POSS_SWy-2. N_2 adsorption–desorption isotherms of SWy-2 (d), POSS_SWy-2 (e) and Cu^{2+}@POSS_SWy-2 (f).

Furthermore, EDS elemental mapping was performed to verify whether the pillaring structures were uniformly distributed and to determine the relative ratio of Cu^{2+} in Cu^{2+}@POSS_SWy-2. As shown in Fig. 3, we collected the EDS spectra in the area marked in dark red in the SEM image (Fig. 3(c)) and found identical spectra, of which one is shown in Fig. 3(d). We then imaged the distribution of Si, Al, N and Cu in the area enclosed in the red square area (Fig. 3(c)) and found a homogeneous distribution for all four elements, which indicates that the insertion of Cu^{2+} into the smectite clay is uniform throughout the sample. In addition, Al and Si are the main components of the smectite layers, which are composed of an octahedral alumina layer and sandwiched between two tetrahedral silica layers. From the elemental composition deduced from the EDS spectra, we can infer that the amount of Cu^{2+} in the nanocomposite is approximately 2.4 wt%.

To estimate the amount of POSS and Cu^{2+}@POSS introduced into SWy-2, TGA-DTA was performed on POSS_SWy-2 and Cu^{2+}@POSS_SWy-2, as well as on the pristine clay; the results are shown in Fig. 4(a–c). For the pristine smectite clay, the broad peak trace observed at 667 °C on the relevant DTA marks the dihydroxylation of structural –OH groups in SWy-2, which make up 3.0% of the total mass.[34] For POSS_SWy-2 and Cu^{2+}@POSS_SWy-2, the region from 200 °C to 500 °C refers to the decomposition of POSS: between 200 °C and 300 °C, amino groups detach from POSS,[35] followed by the combustion of the alkane on the R group of POSS between 300 °C and 500 °C.[21] The Si–O bond decomposition of the POSS-cage and the dehydroxylation of the structural –OH group in SWy-2 occur between 500 °C and 700 °C.[36] From these data, we can estimate that for POSS_SWy-2, the amount of POSS intercalated into SWy-2 equals 2.0 wt% of the total mass, while for Cu^{2+}@POSS_SWy-2, it reaches 8.0 wt% of the total mass. In other words, Cu^{2+} favours the insertion of POSS between SWy-2 layers. If we calculate the amount of nitrogen based on the POSS structure, we find that nitrogen should make up about 2.5 wt% of the total weight, in good agreement with the EDS result (2.6%).

Nitrogen adsorption–desorption measurements were performed on SWy-2, POSS_SWy-2 and Cu^{2+}@POSS_SWy-2 to monitor the increase of surface area with intercalation and to retrieve information on the pore structure; the isotherms are presented in Fig. 4(d–f). As for the pristine smectite, a sudden release of N_2 at $P/P_0 \approx 0.5$ gives rise to a type H3 hysteresis loop, commonly ascribed to slit-shaped pores in layered materials, and the adsorption–desorption isotherm corresponds to a type II isotherm, attributed to the general microporous structure.[37] After POSS and Cu^{2+}@POSS intercalation, the hysteresis loop widens, implying an increase in pore volume from 0.093 $cm^3\ g^{-1}$ in the pristine material to 0.230 $cm^3\ g^{-1}$ in Cu^{2+}@POSS_SWy-2 (Table 1).[38] The specific surface area (SSA) and the pore volume calculated from the BET data are reported in Table 1. The SSA for SWy-2 was found to amount to 26 $m^2\ g^{-1}$, but increased to 127 $m^2\ g^{-1}$ after intercalation with Cu^{2+}@POSS. This indicates that N_2 can only be adsorbed on the external surface and the interlayer space remains inaccessible in the pristine material, while the opening of the interlayer space in the nanocomposite allows for N_2 penetration. However, compared to POSS_SWy-2, a significant increase of SSA can be observed for Cu^{2+}@POSS_SWy-2; this indicates that the Cu^{2+} enhanced POSS intercalation leads to the formation of more mesoporous structures, which can result in a dramatically increased pore surface area.[39]

To gain better insight into the structural characteristics of our materials, we determined the pore size distribution (PSD). For this, the NLDFT method was employed since both micropores and mesopores are present in the structure of pillared smectite clay materials.[40] The PSD results obtained from the NLDFT model are shown in Fig. S2(a),† where one notes that the relative amount of micropores increased with the intercalation of POSS and Cu^{2+}@POSS. The intercalation of POSS in SWy-2 has a limited effect on the internal and external pore distributions.[41] However, when Cu^{2+}@POSS was used as a pillaring agent, the microporosity as well as mesoporosity increased significantly (Fig. S2(b)†). In the micropore range, the peaks in the pore diameter centred at 0.5 nm and 1.4 nm for Cu^{2+}@POSS_SWy-2 differ considerably from the broad peak at 0.7 nm observed when pillaring with POSS.[41] The complexation of Cu^{2+} with the nitrogen-containing ligands results in an increased rigidity of the POSS molecule, which might result in micropores,[42] whose size is centred at 0.5 nm. Since Cu^{2+}@POSS is positively charged, the narrowly distributed pore sizes around 1.4 nm might be the result of electrostatic repulsion.[13] Such electrostatic repulsion could also be responsible for the larger amount of randomly distributed mesopores, giving rise to the hierarchical micro-/mesoporous structure seen in the TEM image, which results in the increase in the total pore volume reported in Table 1.

Adsorption isotherms and adsorption capacity for chloridazon and its metabolites

The adsorption isotherms of chloridazon on SWy-2, POSS_SWy-2 and Cu^{2+}@POSS_SWy-2 are shown in Fig. 5(a).

Table 1 Specific surface area, total pore volume and micropore volume of SWy-2, POSS_SWy-2 and Cu^{2+}@POSS_SWy-2

Samples	Specific surface area (S_{BET}) [$m^2\ g^{-1}$]	Total pore volume [$cm^3\ g^{-1}$]	Micropore volume [$cm^3\ g^{-1}$]
SWy-2	26	0.093	0.004
POSS_SWy-2	54	0.143	0.026
Cu^{2+}@POSS_SWy-2	127	0.230	0.045

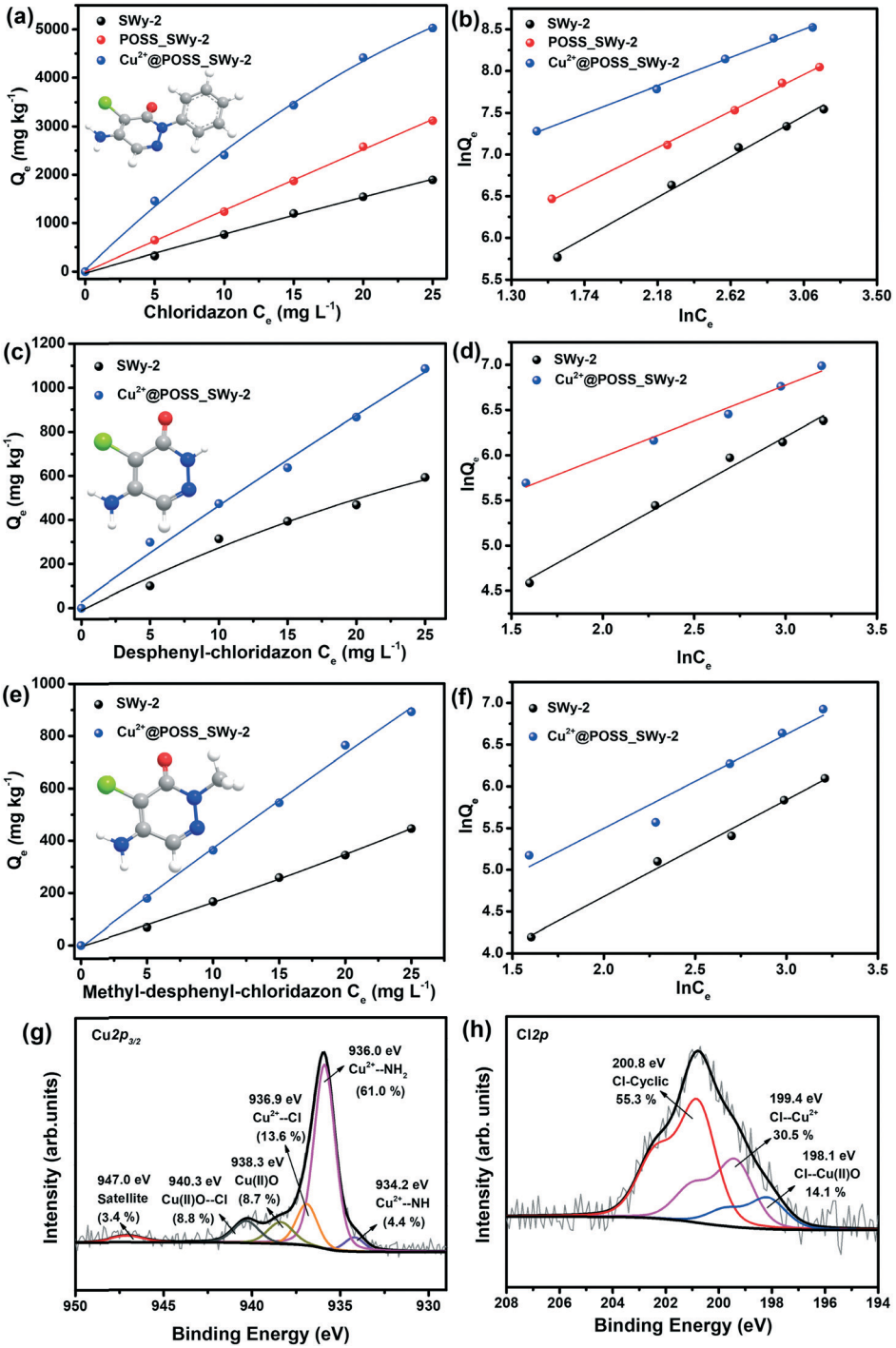

Fig. 5 Adsorption isotherms of (a) chloridazon (inset: structural model of chloridazon; grey = carbon, blue = nitrogen, red = oxygen and green = chlorine), (c) desphenyl-chloridazon (inset: structural model of desphenyl-chloridazon, colour codes same as those in (a)), and (e) methyl-desphenyl-chloridazon (inset: structural model of methyl-desphenyl-chloridazon, colour codes of the balls same as those in (a)). Freundlich model fitting for the adsorption of (b) chloridazon on Cu^{2+}@POSS_SWy-2, POSS_SWy-2 and SWy-2, and Freundlich model fitting for the adsorption of (d) desphenyl-chloridazon and (f) methyl-desphenyl-chloridazon on Cu^{2+}@POSS_SWy-2 and SWy-2. X-ray photoelectron spectra of chloridazon + Cu^{2+}@POSS_SWy-2: (g) $Cu2p_{3/2}$ and (h) Cl2p core level regions.

In the Giles classification, these isotherms can be classified as L-type, which indicates that pristine and intercalated smectite clay materials have a moderate affinity for chloridazon and there is no strong competition from the solvent.[43] However, the slope of the initial part of the adsorption isotherms on Cu^{2+}@POSS_SWy-2 is much higher than on SWy-2, which illustrates that Cu^{2+}@POSS_SWy-2 and POSS_SWy-2 have a higher affinity for chloridazon than SWy-

Table 2 Parameters of Freundlich isotherm model $Q_e = K_f \times C_e^{1/n}$ for the adsorption of chloridazon, desphenyl-chloridazon and methyl-desphenyl-chloridazon on SWy-2, POSS_SWy-2 and Cu^{2+}@POSS_SWy-2

Samples		K_f	n	R^2
Chloridazon	SWy-2	58.22	0.900	0.992
	POSS_SWy-2	137.01	1.008	0.998
	Cu^{2+}@POSS_SWy-2	471.07	1.305	0.996
Desphenyl-chloridazon	SWy-2	17.15	0.892	0.986
	Cu^{2+}@POSS_SWy-2	81.29	1.262	0.984
Methyl-desphenyl-chloridazon	SWy-2	10.55	0.861	0.991
	Cu^{2+}@POSS_SWy-2	25.68	0.934	0.984

2. For an initial concentration of 25 mg L^{-1}, the amount of chloridazon adsorbed on Cu^{2+}@POSS_SWy-2 (Q_e) is nearly 3 times that on SWy-2 and 1.5 times that on POSS_SWy-2. To determine the adsorption capacity of the nanocomposites for chloridazon, the adsorption data were fitted with the Freundlich model and the result is shown in Fig. 5(b). The fit and the statistical analysis were performed with Origin software and the estimated parameters are given in Table 2. K_f is an empirical constant related to the adsorption capacity ($mg^{(1-n)}$ kg^{-1} L^n), n is the Freundlich exponent or a site energy heterogeneity factor, often used as a measure of isotherm nonlinearity,[44] and the value of the correlation coefficient R^2 relates to the quality of the isotherm fit: the closer the value to 1, the better the fit. As can be seen from Table 2, R^2 values amounted to 0.992, 0.998 and 0.996 for SWy-2, POSS_SWy-2 and Cu^{2+}@POSS_SWy-2, confirming a good fit in all cases. The empirical constant K_f increased 8 times for the adsorption of chloridazon on Cu^{2+}@POSS_SWy-2 compared to that for adsorption on the pristine clay. The higher adsorption capacity of Cu^{2+}@POSS_SWy-2 can be ascribed to two reasons: on the one hand, the significantly higher specific surface area of Cu^{2+}@POSS_SWy-2 provides more physisorption sites for chloridazon. On the other hand, the presence of Cu^{2+}, which has a strong affinity for Cl- and N-containing organic molecules, enhances the chemisorption of chloridazon.

In order to check the adsorption mechanism of chloridazon on Cu^{2+}@POSS_SWy-2, XPS was performed. As shown in Fig. 5(g), the $Cu2p_{3/2}$ core-level region requires 5 components in the fit. The three components also present in the starting material, *i.e.* the first one due to Cu^{2+}–NH at a BE of 934.2 eV, the second one stemming from Cu^{2+}–NH_2 at 936.0 eV and the third originating from Cu(II)O at 938.3 eV,[33,45] contribute here differently to the $Cu2p_{3/2}$ spectral intensity. The increased relative intensity of the Cu^{2+}–NH_2 component (now 61.0%) and the decreased relative intensity of the Cu^{2+}–NH one (now 4.4%) confirm that the –NH_2 group of chloridazon is very active towards Cu^{2+} and replaces the weakly bonded –NH group. Additionally, the two new components at BEs of 936.9 eV and 940.3 eV can be ascribed to the adsorption of Cl to Cu^{2+} and Cu(II)O, respectively. In fact, since the –Cl group of chloridazon is more electronegative than –NH_2, Cu^{2+} to which it is attached becomes more electron-poor, and hence appears at a higher BE.[45] Likewise, –Cl attached to Cu(II)O further decreases the electron density around the Cu^{2+}, resulting in an additional component at a higher binding energy.[33] Correspondingly, the Cl2p core-level region (Fig. 5(h)) can be fitted with three components at BEs of 198.1 eV, 199.4 eV and 200.8 eV and originating respectively from Cl–Cu(II)O,[46] Cl–Cu^{2+},[45] and Cl-cyclic of chloridazon.[47] The N1s core level region, reported in the ESI,† agrees with this interpretation.

The uptake of desphenyl-chloridazon on Cu^{2+}@POSS_SWy-2 was also found to be significantly higher than that on SWy-2, as seen from the adsorption isotherms shown in Fig. 5(c). At an initial concentration of 25 mg L^{-1}, the Q_e for desphenyl-chloridazon adsorbed on Cu^{2+}@POSS_SWy-2 is nearly 2 times that on SWy-2. The Freundlich model fitting results are shown in Fig. 5(d) and the data are listed in Table 2. Similar to chloridazon, also for desphenyl-chloridazon, the empirical constant K_f significantly increased for adsorption on Cu^{2+}@POSS_SWy-2 as compared to pristine SWy-2, and the Freundlich exponent n changed from 0.892 to 1.262, testifying to an improved adsorption capacity.

For the uptake of the other metabolite, methyl-desphenyl-chloridazon, the isotherms are shown in Fig. 5(e) and their fit with the Freundlich model is shown in Fig. 5(f). Since methyl-desphenyl-chloridazon and desphenyl-chloridazon have a similar chemical structure, their adsorption behaviour is analogous. At an initial concentration of 25 mg L^{-1}, the Q_e for methyl-desphenyl-chloridazon on Cu^{2+}@POSS_SWy-2 was determined to amount to 891 mg kg^{-1}, which is twice that on SWy-2. The observed difference between the uptake of chloridazon, desphenyl-chloridazon and methyl-desphenyl-chloridazon is attributed to the different substituent group at the imino position. The significantly higher uptake capacity for chloridazon than those for its two metabolites is presumably related to the phenyl group. On the one hand, the higher adsorption capacity can be ascribed to the hydrophobic effects because the siloxanes of the basal planes are considered to be hydrophobic, and therefore have a higher affinity for organic molecules containing aromatic rings.[48] This type of bonding is not present for desphenyl-chloridazon and methyl-desphenyl-chloridazon, where the phenyl group is replaced by hydrogen or by a methyl group. On the other hand, the phenyl group is electron richer than –CH_3 or –H, which means it can donate more electronic charges to –NH_2 and –Cl to make them more electronegative than in desphenyl-chloridazon and methyl-desphenyl-

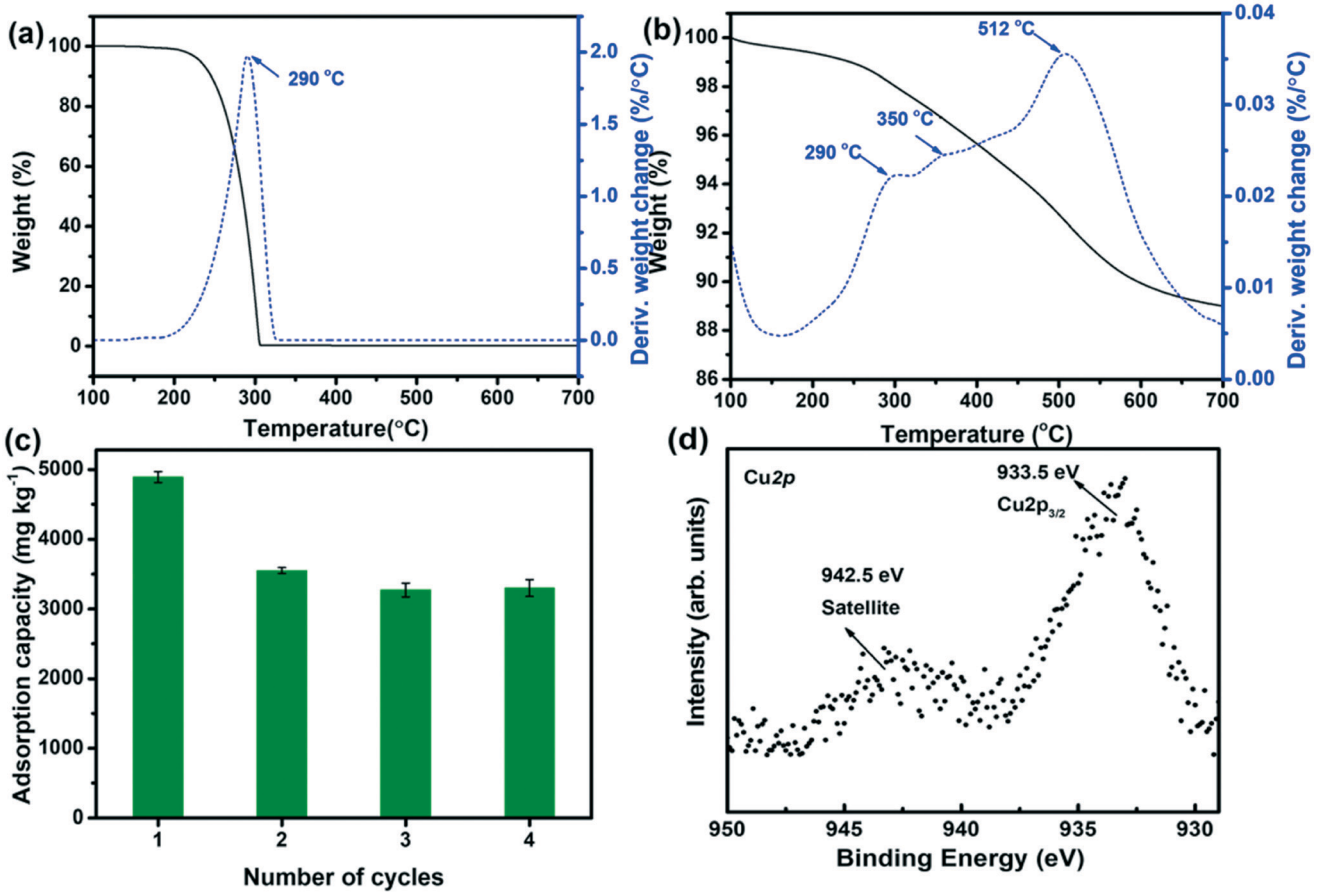

Fig. 6 Thermogravimetric analysis (TGA) and differential thermal analysis (DTA) data for (a) chloridazon and (b) Cu^{2+}@POSS_SWy-2 + chloridazon, and (c) adsorption capacity for chloridazon of Cu^{2+}@POSS_SWy-2 after an increasing number of thermal regeneration cycles. (d) X-ray photoelectron spectrum of the $Cu2p_{3/2}$ core level region of thermally regenerated Cu^{2+}@POSS_SWy-2.

chloridazon. This results in Cu^{2+} having a relatively higher affinity for chloridazon.

Thermal regeneration analysis

An important issue for assessing the potential of Cu^{2+}@POSS_SWy-2 as a chloridazon adsorbent is to test its reusability; hence we regenerated the material thermally and followed the sorption behaviour over four adsorption/regeneration cycles. The TGA/DTA data for chloridazon, presented in Fig. 6(a), show that decomposition occurs around 290 °C. However, as discussed above (Fig. 6(b)), below 300 °C, the amino groups detach from POSS, while Cu^{2+} remains in the interlayer space of SWy-2. This means that after decomposition of the adsorbed chloridazon at 290 °C, the structure of Cu^{2+}@POSS_SWy-2 is slightly altered, but the pillaring Si–O cubes still remain intact. We therefore checked if the material still adsorbs chloridazon after this regeneration treatment. The adsorption capacity of Cu^{2+}@POSS_SWy-2 for chloridazon as a function of number of regeneration cycles is plotted in Fig. 6(c). While the pristine Cu^{2+}@POSS_SWy-2 adsorbs 4920 ± 36 mg kg^{-1}, after four thermal regeneration cycles, the adsorption capacity for chloridazon was 3260 ± 61 mg kg^{-1}, *i.e.* reduced by 32.3%. To check whether this reduction is due to the oxidation of Cu^{2+} to Cu(II)O, which weakens the affinity for chloridazon, we checked the XPS spectrum of the $Cu2p_{3/2}$ core level region of thermally regenerated Cu^{2+}@POSS_SWy-2, as shown in Fig. 6(d). The spectrum clearly testifies to an important increase of Cu(II)O after the heat treatment.[32,33] Despite this decrease in adsorption capacity after recycling, Cu^{2+}@POSS_SWy-2 can be considered as a potential adsorbent for chloridazon and its metabolites.

Conclusions

We established a controllable and reproducible synthesis method for a new adsorbent of chloridazon and its metabolites, namely smectite clay pillared with copper complexed polyhedral oligosilsesquioxane. The successful intercalation of Cu^{2+} complexed POSS into the interlayer space of the clay was confirmed by FTIR, XRD and high-resolution TEM. X-ray photoelectron spectroscopy as well as thermogravimetric and differential thermal analysis illustrated the type of interaction between the host materials and the intercalated molecules, and also shed light on the

intercalation yield. Porosimetry measurements revealed that pillared structures are created and gave the specific surface area of the hybrid nanostructures. The hybrid nanostructure obtained by intercalation of Cu^{2+}@POSS into the smectite clay showed a four times higher adsorption capacity for chloridazon, and a two times higher adsorption capacity for its metabolites, desphenyl-chloridazon and methyl-desphenyl-chloridazon, than the pristine SWy-2. This enhanced performance is attributed to the high specific surface area and the affinity of copper ions for nitrogen-containing herbicides. Cu^{2+}@POSS_SWy-2 maintains an excellent adsorption capacity even after several thermal regeneration cycles. These findings show the potential of Cu^{2+}@POSS_SWy-2 as a relatively low cost material for herbicide waste remediation.

Author contributions

D. Gournis and P. Rudolf designed the experiments and finalized the manuscript. F. Yan conducted all the experiments and wrote the draft of the manuscript. K. Spyrou and E. Thomou participated in the synthesis, S. Kumar participated in the XPS experiments and in the analysis of the XPS data, H. Cao and Y. Pei participated in the SEM experiments, and M. C. A. Stuart conducted the TEM experiments and participated in the analysis of the data. All authors discussed the results and commented on the manuscript.

Conflicts of interest

There are no conflicts to declare.

Acknowledgements

F. Y. thanks the China Scholarship Council (CSC No. 201704910930) and the University of Groningen for support for his PhD studies. E. T. was supported by the Hellenic Foundation for Research and Innovation (HFRI) and the General Secretariat for Research and Technology (GSRT), under the HFRI PhD Fellowship grant (GA. no. 1829). This work was supported by the Advanced Materials research program of the Zernike National Research Centre under the Bonus Incentive Scheme of the Dutch Ministry for Education, Culture and Science.

Notes and references

1 H. Yang, R. Bain, J. Bartram, S. Gundry, S. Pedley and J. Wright, Water safety and inequality in access to drinking-water between rich and poor households, *Environ. Sci. Technol.*, 2013, **47**, 1222–1230.
2 J. Wu and Z. Sun, Evaluation of Shallow Groundwater Contamination and Associated Human Health Risk in an Alluvial Plain Impacted by Agricultural and Industrial Activities, Mid-west China, *Exposure Health*, 2016, **8**, 311–329.
3 D. Lapworth, N. Baran, M. Stuart and R. Ward, Emerging organic contaminants in groundwater: a review of sources, fate and occurrence, *Environ. Pollut.*, 2012, **163**, 287–303.
4 T. Reemtsma, L. Alder and U. Banasiak, Emerging pesticide metabolites in groundwater and surface water as determined by the application of a multimethod for 150 pesticide metabolites, *Water Res.*, 2013, **47**, 5535–5545.
5 E. Jakiene, V. Spruogis, A. Dautarte, K. Romaneckas and D. Avizienyte, The bio-organic nano fertilizer improves sugar beet photosynthesis process and productivity, *Zemdirbyste*, 2015, **102**, 141–146.
6 G. Buttiglieri, M. Peschka, T. Frömel, J. Müller, F. Malpei, P. Seel and T. P. Knepper, Environmental occurrence and degradation of the herbicide n-chloridazon, *Water Res.*, 2009, **43**, 2865–2873.
7 GWD, EU. Directive 2006/118/EC of the European Parliament and of the Council of 12 December 2006 on protection of groundwater against pollution and deterioration. O. J. L, 2006, vol. 372, pp. 19–31.
8 A. Schuhmann, O. Gans, S. Weiss, J. Fank, G. Klammler, G. Haberhauer and M. H. Gerzabek, A long-term lysimeter experiment to investigate the environmental dispersion of the herbicide chloridazon and its metabolites-comparison of lysimeter types, *J. Soils Sediments*, 2016, **16**, 1032–1045.
9 A. Alsbaiee, B. J. Smith, L. Xiao, Y. Ling, D. E. Helbling and W. R. Dichtel, Rapid removal of organic micropollutants from water by a porous β-cyclodextrin polymer, *Nature*, 2016, **529**, 190.
10 F. Bergaya and G. Lagaly. General introduction: clays, clay minerals, and clay science, in *Handbook of clay science: Developments in clay science*, 2006, vol. 1, pp. 1–18.
11 D. Carroll, Ion exchange in clays and other minerals, *Geol. Soc. Am. Bull.*, 1959, **70**, 749–779.
12 M. Auta and B. Hameed, Modified mesoporous clay adsorbent for adsorption isotherm and kinetics of methylene blue, *Chem. Eng. J.*, 2012, **198**, 219–227.
13 T. Pinnavaia, Intercalated clay catalysts, *Science*, 1983, **220**, 365–371.
14 C. W. Chiu, T. K. Huang, Y. C. Wang, B. G. Alamani and J. J. Lin, Intercalation strategies in clay/polymer hybrids, *Prog. Polym. Sci.*, 2014, **39**, 443–485.
15 B. Krishna, D. Murty and B. J. Prakash, Surfactant-modified clay as adsorbent for chromate, *Appl. Clay Sci.*, 2001, **20**, 65–71.
16 J. Luo, W. Zhang, H. Yuan, C. Jin, L. Zhang, H. Huang, C. Liang, Y. Xia, J. Zhang and Y. Gan, Pillared structure design of MXene with ultralarge interlayer spacing for high-performance lithium-ion capacitors, *ACS Nano*, 2017, **11**, 2459–2469.
17 D. M. Fox, P. H. Maupin, R. H. Harris, J. W. Gilman, D. V. Eldred, D. Katsoulis, P. C. Trulove and H. C. De Long, Use of a polyhedral oligomeric silsesquioxane (POSS)-imidazolium cation as an organic modifier for montmorillonite, *Langmuir*, 2007, **23**, 7707–7714.
18 F. Carniato, C. Bisio, G. Gatti, E. Boccaleri, L. Bertinetti, S. Coluccia, O. Monticelli and L. Marchese, Thermal stability of

polystyrene nanocomposites from improved thermally stable organoclays, *Angew. Chem., Int. Ed.*, 2009, **48**, 6059–6061.

19 G. Potsi, A. Rossos, A. Kouloumpis, M. Antoniou, K. Spyrou, M. A. Karakassides, D. Gournis and P. Rudolf, Carbon nanostructures containing polyhedral oligomeric silsesquioxanes (POSS), *Curr. Org. Chem.*, 2016, **20**, 662–673.

20 H. He, B. Li, J. Dong, Y. Lei, T. Wang, Q. Yu, Y. Feng and Y. Sun, Mesostructured nanomagnetic polyhedral oligomeric silsesquioxanes (POSS) incorporated with dithiol organic anchors for multiple pollutants capturing in wastewater, *ACS Appl. Mater. Interfaces*, 2013, **5**, 8058–8066.

21 G. Potsi, A. K. Ladavos, D. Petrakis, A. P. Douvalis, Y. Sanakis, M. S. Katsiotis, G. Papavassiliou, S. Alhassan, D. Gournis and P. Rudolf, Iron-substituted cubic silsesquioxane pillared clays: Synthesis, characterization and acid catalytic activity, *J. Colloid Interface Sci.*, 2018, **510**, 395–406.

22 D. Gournis, A. Lappas, M. Karakassides, D. Többens and A. Moukarika, A neutron diffraction study of alkali cation migration in montmorillonites, *Phys. Chem. Miner.*, 2007, **35**, 49–58.

23 D. Petridis, D. Gournis and M. Karakassides, The Chemistry of Organofunctionalized Silicon Cubanes in Swelling Smectites, *Mol. Cryst. Liq. Cryst.*, 2006, **311**, 345–350.

24 P. Olivera-Pastor, P. Mairles-Torres, E. Rodriguez-Castellon and A. Jimenez-Lopez, Nanostructured inorganically pillared layered metal (IV) phosphates, *Chem. Mater.*, 1996, **8**, 1758.

25 J. Landers, G. Gennady and N. Alexander, Density functional theory methods for characterization of porous materials, *Colloids Surf., A*, 2013, **437**, 3–32.

26 O. Ivashenko, H. Logtenberg, J. Areephong, A. Coleman, P. Wesenhagen, E. Geertsema, N. Heureux, B. L. Feringa, P. Rudolf and W. Browne, Remarkable stability of high energy conformers in self-assembled monolayers of a bistable electro-and photoswitchable overcrowded alkene, *J. Phys. Chem. C*, 2011, **115**, 22965–22975.

27 T. L. Barr, An XPS study of Si as it occurs in adsorbents, catalysts, and thin films, *Appl. Surf. Sci.*, 1983, **15**, 1–35.

28 M. A. Karakassides, D. Gournis and D. Petridis, An infrared reflectance study of Si–O vibrations in thermally treated alkali-saturated montmorillonites, *Clay Miner.*, 1999, **34**, 429–438.

29 K. Spyrou, G. Potsi, E. K. Diamanti, X. Ke, E. Serestatidou, I. I. Verginadis, A. P. Velalopoulou, A. M. Evangelou, Y. Deligiannakis, G. Van Tendeloo, D. Gournis and P. Rudolf, Towards novel multifunctional pillared nanostructures: Effective intercalation of adamantylamine in graphene oxide and smectite clays, *Adv. Funct. Mater.*, 2014, **24**, 5841–5850.

30 K. G. Theng, *The Chemistry of Clay-Organic Reactions*, Adam Hilger, London, 1974, p. 133.

31 G. Balomenou, P. Stathi, A. Enotiadis, D. Gournis and Y. Deligiannakis, Physicochemical study of amino-functionalized organosilicon cubes intercalated in montmorillonite clay: H-binding and metal uptake, *J. Colloid Interface Sci.*, 2008, **325**, 74–83.

32 J. Huo, X. Liu, X. Li, L. Qin and S. Z. Kang, An efficient photocatalytic system containing Eosin Y, 3D mesoporous graphene assembly and CuO for visible-light-driven H2 evolution from water, *Int. J. Hydrogen Energy*, 2017, **42**, 15540–15550.

33 S. Poulston, P. M. Parlett, P. Stone and M. Bowker, Surface Oxidation and Reduction of CuO and Cu_2O Studied Using XPS and XAES, *Surf. Interface Anal.*, 1996, **24**, 811–820.

34 R. Mansa, L. Dzene, A. Quintela, F. Rocha and C. Detellier, Preparation and characterization of novel clay/scleroglucan nanocomposites, *Appl. Clay Sci.*, 2016, **126**, 235–244.

35 I. Weiss, C. Muth, R. Drumm and H. O. K. Kirchner, Thermal decomposition of the amino acids glycine, cysteine, aspartic acid, asparagine, glutamic acid, glutamine, arginine and histidine, *BMC Biophys.*, 2018, **11**, 1–2.

36 F. Zhao, C. Wan, X. Bao and B. Kandasubramanian, Modification of montmorillonite with aminopropylisooctyl polyhedral oligomeric silsequioxane, *J. Colloid Interface Sci.*, 2009, **333**, 164–170.

37 O. Cubuk, C. Bulent, T. Cihan, C. Fatih, S. Gokhan, T. Ahmet and S. Erdal, Structural characterization of hexadecyl-trimethylammonium-smectite composites and their potentiometric electrode applications, *Appl. Surf. Sci.*, 2015, **338**, 99–112.

38 K. Kaneko, Determination of pore size and pore size distribution: 1. Adsorbents and catalysts, *J. Membr. Sci.*, 1994, **96**, 59–89.

39 D. Chen, G. Du, Q. Zhu and F. Zhou, Synthesis and characterization of TiO2 pillared montmorillonites: application for methylene blue degradation, *J. Colloid Interface Sci.*, 2013, **409**, 151–157.

40 P. Behrens, Mesoporous inorganic solids, *Adv. Mater.*, 1993, **5**, 127–132.

41 M. E. R. Jalil, R. Vieira, D. Azevedo, M. Baschini and K. Sapag, Improvement in the adsorption of thiabendazole by using aluminum pillared clays, *Appl. Clay Sci.*, 2013, **71**, 55–63.

42 M. Opanasenko, W. Parker Jr, M. Shamzhy, E. Montanari, M. Bellettato, M. Mazur, R. Millini and J. Čejka, Hierarchical hybrid organic–inorganic materials with tunable textural properties obtained using Zeolitic-layered precursor, *J. Am. Chem. Soc.*, 2014, **136**, 2511–2519.

43 C. Giles, D. Smith and A. Huitson, A general treatment and classification of the solute adsorption isotherm. I. Theoretical, *J. Colloid Interface Sci.*, 1974, **47**, 755–765.

44 N. Daneshvar, S. Aber, A. Khani and M. Rasoulifard, Investigation of adsorption kinetics and isotherms of imidacloprid as a pollutant from aqueous solution by adsorption onto industrial granular activated carbon, *J. Food, Agric. Environ.*, 2007, **5**, 425.

45 D. Drolet, D. Manuta, A. Lees, A. Katnani and G. Coyle, FT-IR and XPS study of copper (II) complexes of imidazole and benzimidazole, *Inorg. Chim. Acta*, 1988, **146**, 173–180.

46 J. Ci, W. Tu, W. Uen, S. Lan, J. Zeng, T. Yang, C. Shen and J. Jhao, Chlorine-doped n-type cuprous oxide films fabricated

by chemical bath deposition, *J. Electrochem. Soc.*, 2014, **161**, D321–D326.

47 T. Mondal, A. Bhowmick and R. Krishnamoorti, Chlorophenyl pendant decorated graphene sheet as a potential antimicrobial agent: synthesis and characterization, *J. Mater. Chem.*, 2012, **22**, 22481–22487.

48 J. Lambert, Organic pollutant adsorption on clay minerals, *Dev. Clay Sci.*, 2018, **9**, 195–253.